第 49 卷第 9 期
2021 年 9 月

硅 酸 盐 学 报
JOURNAL OF THE CHINESE CERAMIC SOCIETY

Vol. 49，No. 9
September，2021

http://www.gxyb.cbpt.cnki.net

DOI：10.14062/j.issn.0454-5648.20200920

四方钨青铜结构 $NaSr_2Nb_5O_{15}$ 铁电陶瓷的致密化

吕 蕊，刘亮亮，王永强

(太原理工大学材料科学与工程学院，太原 030024)

摘 要：以 TTB 结构的 $NaSr_2Nb_5O_{15}$ (NSN)为研究对象，采用常规固相烧结法合成的 NSN 和中间体($NaNbO_3$ 和 $SrNb_2O_6$)粉体作为基体，利用熔盐法合成大尺寸的 NSN 微晶作为晶种。通过原料设计，制备出致密的 NSN 陶瓷。研究了晶种含量对 NSN 陶瓷烧结行为和微观组织的影响。结果表明：在基体中加入晶种，通过反应烧结可以制备出致密的 NSN 陶瓷；随着晶种含量的增加，NSN 陶瓷的微观组织结构发生明显变化。

关键词：铌酸锶钠；致密化；微观结构；无铅陶瓷
中图分类号：TQ174　　**文献标志码**：A　　**文章编号**：0454–5648(2021)09–1943–09
网络出版时间：2021–07–30



Densification of $NaSr_2Nb_5O_{15}$ Ferroelectric Ceramics with Tetragonal Tungsten Bronze Structures

LV Rui, *LIU Liangliang*, *WANG Yongqiang*
(College of Materials Science and Engineering, Taiyuan University of Technology, Taiyuan 030024, China)

Abstract: Ceramics with tetragonal tungsten bronze (TTB)-type structures undoped with sintering aids are difficult to densify due to the high anisotropy of their crystal structures. In this paper, TTB-structured $NaSr_2Nb_5O_{15}$ (NSN) was selected as the research object to prepare dense ceramics by the design of raw materials. Two powders synthesized by conventional solid-state sintering and molten salt methods were used. The former powder consisted of three phases as the matrix, NSN and intermediate phases ($NaNbO_3$ and $SrNb_2O_6$). The latter powder, with a large particle size, acted as a seed. The effects of seed content on the sintering behavior and microstructure of NSN ceramics were investigated. Dense NSN ceramics were prepared by reaction sintering using seed addition into the matrix. The seed content had an obvious influence on the microstructures of the NSN ceramics.

Keywords: sodium niobate strontium; densification; microstructure; lead-free ceramics

1 Introduction

At present, lead-free piezoelectric ceramics have attracted considerable attention as candidate materials to replace Pb-based ceramics due to environmental-protection and human-health concerns[1–5]. Among these candidate materials, tungsten bronze compounds have been extensively studied owing to their excellent dielectric, electro-optic, piezoelectric, and ferroelectric properties[6–10]. With the rapid advancement of textured ceramics, tetragonal tungsten bronze (TTB)-type compounds have become an exciting class of materials because of their substantial anisotropy of piezoelectric properties[11–12] and the easy synthesis of crystallites with high aspect ratios[13–15]. The TTB structure can be described by the general formula $(A1)_4(A2)_2C_4(B)_{10}O_{30}$. This structure is typified by oxygen octahedra sharing their corners in a sophisticated way to create three different types of cavities, *e.g.*, square, pentagonal, and triangular tunnels available for cation inclusion (denoted

收稿日期：2020–12–15。　修订日期：2021–02–05。
基金项目：国家自然科学基金项目(51502191)资助。
第一作者：吕 蕊(1994—)，男，硕士研究生。
通信作者：刘亮亮(1985—)，男，讲师。

Received date: 2020–12–15.　**Revised date:** 2021–02–05.
First author: LV Rui (1994–), male, Master candidate.
E-mail: lvrui_031018@163.com
Correspondent author: LIU Liangliang (1985–), male, Ph.D, Lecturer.
E-mail: liuliangliang_2004@163.com

hereafter *A*1, *A*2, and *C* sites, respectively). The sizes of these cavities decrease in the order *A*2>*A*1>*C*. While the terms "filled" and/or "unfilled" TTB structure are frequently applied in the literature, these terms are independent of the small C site. That is, only if all *A* (*A*1 and *A*2) sites are occupied does this situation represent 'filled' TTB structures; otherwise, the structure is called an 'unfilled' TTB. As a representative filled TTB structural system, $NaSr_2Nb_5O_{15}$ (NSN) ceramics have shown great development potential. To date, although random[16–21] and textured NSN ceramics[18] have been obtained by various methods, these investigations have been focused on the promotion of electrical performance. Limited attention in the literature has been given to the densification behavior of ceramics. The densification behavior of ceramics in tungsten bronze oxides is still not well understood. It has been reported that a second phase could be easily generated during the sintering process of NSN ceramics[22]. Moreover, this TTB structure exhibited high anisotropy, leading to cracking and abnormal grain growth during the sintering process[23]. As a result, it was difficult to prepare dense NSN ceramics using conventional solid-state sintering methods. This also makes it difficult to develop the electrical properties of NSN ceramics. To date, various strategies have been adopted to improve the density of NSN ceramics, such as the sol–gel method[24], wet chemical techniques[25], and the two-step solid-state reaction method[21]. Although these methods improved the electrical properties of ceramics, the high production costs and complex preparation processes have limited their widespread usage in piezoelectric devices. In addition, addition of a sintering aid was also an effective method to promote the densification of NSN ceramics[18]. However, these additives might deteriorate the electrical properties, according to related reports[23–26]. Based on previous simulation and experimental results[27–28], densification could be facilitated by using the (reactive) template grain growth method. It has been reported that the densities of ceramics were significantly increased by adding needle-like $KSr_2Nb_5O_{15}$ microcrystals as seeds[29–30]. However, the addition of KSN seeds inevitably caused the diffusion of K^+ into the NSN lattice[18]. In our previous work, acicular NSN particles with good dispersion were synthesized by the molten salt synthesis (MSS) method[31–32]. NSN has the same phase structure as KSN, and the difference in lattice parameters in the *a* and *c* directions was 0.01, as indicated by JCPDS Cards (No. 34-0 108 and No. 34-0 429). Therefore, it is reasonable to expect that high-density NSN ceramics could be synthesized by adding NSN seeds.

NSN seeds and matrix powder were employed to fabricate NSN ceramics by the reaction sintering method. The effects of seed contents on the phase formation and microstructure development, as well as the electrical properties of ceramics, were investigated. A special emphasis was placed on the sintering behavior of ceramics.

2 Experimental

$NaSr_2Nb_5O_{15}$ (NSN) ceramics were prepared by reaction sintering of the matrix and seed powder. The synthesis of matrix powder (NSN powder and intermediates) requires two steps in the conventional mixed-oxide (CMO) method. First, the intermediates $SrNb_2O_6$ and $NaNbO_3$ were obtained by heating stoichiometric mixtures of $SrCO_3$ (99.0%)–Nb_2O_5 (99.99%) and K_2CO_3 (99.0%)–Nb_2O_5 (99.99%) at 1 100 ℃ for 4 h and 780 ℃ for 3 h, respectively. Then, matrix particles were synthesized by heating the stoichiometric intermediates ($SrNb_2O_6$+$NaNbO_3$) at 1 220 ℃ for 6 h. The seed particles were obtained by an MSS method. Further details of the synthesis of the seed particles have been reported previously[32]. High purity Nb_2O_5 (99.99%), $SrCO_3$ (99.0%), KCl (99.5%) and NaCl (99.5%) were selected as raw materials. The weight ratio of salts (NaCl+KCl) to oxides (Nb_2O_5+Sr_2CO_3) was 5, and the molar ratio of NaCl/KCl=1. Stoichiometric amounts of the starting powders were mixed for 8 h in a polypropylene jar with ZrO_2 balls (as grinding media) in ethanol. After drying, these powders were placed into an alumina crucible with a flat lid to inhibit the evaporation of KCl and NaCl. Then, the crucible was heated to 1 220 ℃ for 6 h in air. After calcination, the resulting particles were washed several times with hot deionized water to ensure complete removal of the residual KCl and NaCl salts.

The mixtures (matrix and seed) were combined by using ball milling with zirconia balls (as grinding media) in ethanol for 8 h. The designed system in this work was matrix+*x*NSN seed, designated as *x*NSN, where *x* is the mass fraction of seed (0, 0.1, 0.2, 0.4, 0.6, 0.8 and 1), *e.g.*, 0NSN, 0.1NSN, 0.2NSN, 0.4NSN, 0.6NSN, 0.8NSN, and NSN. After drying, the mixture was granulated with PVA binder and then pressed into pellets with a diameter of 12 mm and thickness of 1.3 mm under a pressure of approximately 10 MPa for 30 s. The pellets were heated at 500 ℃ for 2 h to burn out the binder. Subsequently, all green disks were sintered by heating up to 1 280 ℃ with a heating rate of 5 ℃/min, kept at the temperature for 2 h, and cooled to room temperature at a rate of 2 ℃/min. Silver electrodes were coated on both faces of each ceramic sample, and they were calcined at 650 ℃ for 10 min.

The bulk densities of the sintered specimens were determined by using the Archimedes method, and 5.038 $g \cdot cm^{-3}$ was used to calculate the relative density of the NSN ceramics. The phase structures of the powders and ceramics were determined by X-ray diffraction (XRD) (UltimalV, Rigaku, Japan) using Cu K_α radiation and a graphite monochromator. The lattice constants were calculated by software (MDI Jade 6.1, Materials Data Inc, America). Particle morphologies were characterized

by scanning electron microscopy (MIRAS XMH, Tescan, Czech Republic). The microstructures of the polished surfaces of the ceramics were examined by scanning electron microscopy (JSM-IT200, Jeol Ltd, Japan) and a focused ion beam cutter (LYRA3 XMH, Tescan, Czech Republic). The temperature and frequency dependence of the dielectric constant (ε) and dielectric loss (tanδ) were measured on an LCR precision electric meter (HP 4 284, Hewlett-Packard, Palo Alto, Canada) over a temperature range of –150 ℃ to 350 ℃ at different frequencies (1 kHz, 10 kHz and 100 kHz). Ferroelectric hysteresis loops (*P*-*E* loop) were measured at room temperature using a precision materials analyzer (RT66, Radiant Technology, USA). The piezoelectric coefficient (d_{33}) of the poled samples was measured by using a quasi-static piezoelectric d_{33} meter (ZJ-3AN, Institute of Acoustics, Academia Sinica, China).

3 Results and discussion

3.1 Synthesis of matrix and seed powder

In previous research, Li *et al*.[22] reported that the reaction sintering method was conducive to the densification of NSN ceramics. However, the preparation of TTB structure ceramics by this method may result in abnormal grain growth in the case of seed addition[26]. Therefore, in this work, we believed that it was necessary to synthesize a matrix mixture of NSN powder and intermediates ($SrNb_2O_6$ and $NaNbO_3$) by adjusting the process parameters. For the synthesis of the matrix by the CMO method, the intermediates $NaNbO_3$ and $SrNb_2O_6$ were required. Fig. 1 shows the XRD patterns of the synthesized intermediates. As shown in Fig. 1(a), the major diffraction peaks of the products fit well with Joint Committee on Powder Diffraction Standards Card No. 74-2 455, indicating the formation of perovskite-type oxide $NaNbO_3$. Additionally, a small amount of impurity was observed, which was assigned to $Na_2Nb_4O_{11}$. The formation of the $Na_2Nb_4O_{11}$ phase could be attributed to further reaction between the desired $NaNbO_3$ and Nb_2O_5. Fig. 1(b) shows that all XRD diffraction peaks could be readily indexed to cubic $SrNb_2O_6$ with no secondary phase.

Fig. 2 shows the XRD patterns and SEM micrographs of the matrix and seed synthesized by the CMO and MSS methods, respectively. A comparison of Figs. 2(a) and 2(b) indicated that the synthetic method had a crucial influence on the morphology of the powder. The matrix powder showed equiaxial morphology, and the average size was approximately 2 μm. The seed powder showed an acicular morphology with good dispersion, and the average aspect ratio of the particles reached 7.5, which was an ideal template for the preparation of textured NSN ceramics. As shown in Fig. 2(c), it was found that all major peaks of the matrix powder could be assigned to a tetragonal tungsten bronze phase of NSN according to PDF No. 34-0 429. Additionally, the remaining

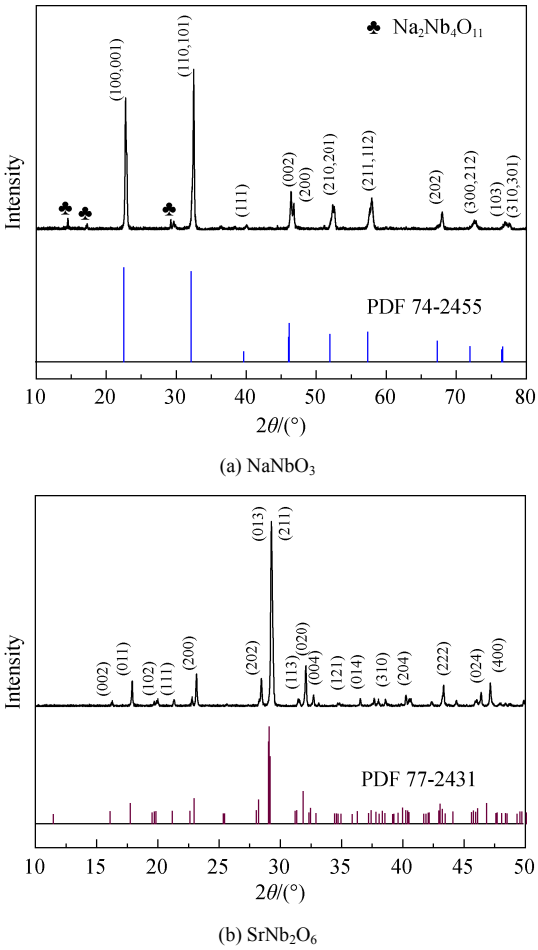
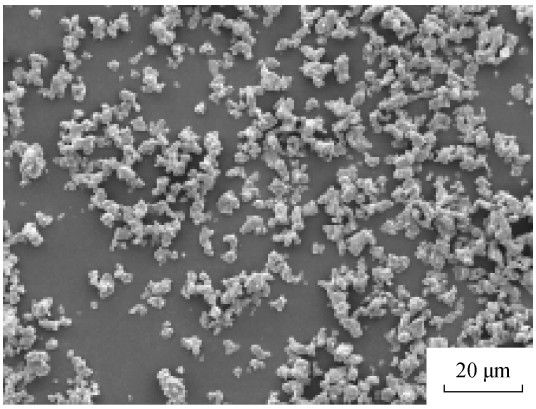
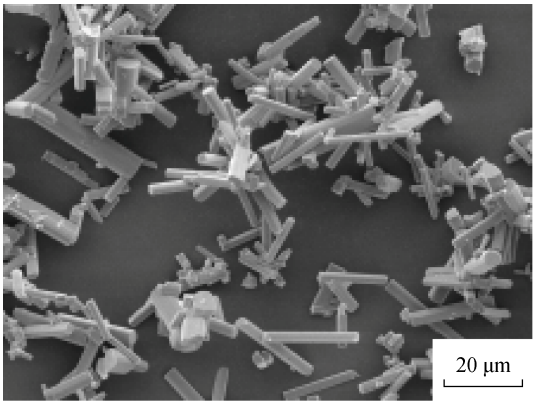


Fig. 1　XRD patterns of the intermediate powder obtained by the CMO method.

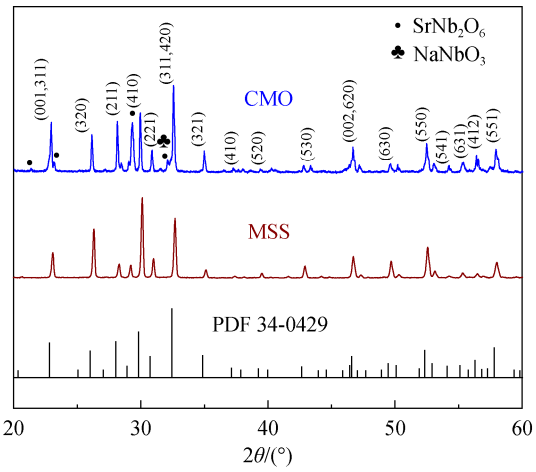
diffraction peaks indexed well with intermediate phases ($NaNbO_3$ and $SrNb_2O_6$). These intermediate phases provided conditions for reaction sintering during the preparation of ceramics. Similarly, all diffraction peaks of the seed powder could be assigned to a tetragonal phase of NSN, and no second phase was detected. It is worth mentioning that all major diffraction peaks were shifted toward smaller 2θ values compared with the standard PDF card. This result was consistent with other studies[20]. This might be attributed to the substitution of Sr^{2+} by the larger Na^+ ($r(Sr^{2+})$=0.113 nm, $r(Na^+)$=0.139 nm). Moreover, although both of the samples exhibited a tetragonal phase of NSN, the intensities of the diffraction peaks indexed to the same crystal plane were significantly different. The most intense peak corresponding to the matrix powder was (311)/(420), which was consistent with the standard PDF card. The most intense peak corresponding to the seed powder became (410), indicating that the surface energy of the (001) plane in the TTB crystal was higher than those of the other planes, and the surface of the particles was parallel to the [001] direction. It has been widely accepted that the growth rate of a crystal depends on the free energy of each surface. The reduction in the total



(a) Matrix



(b) Seed



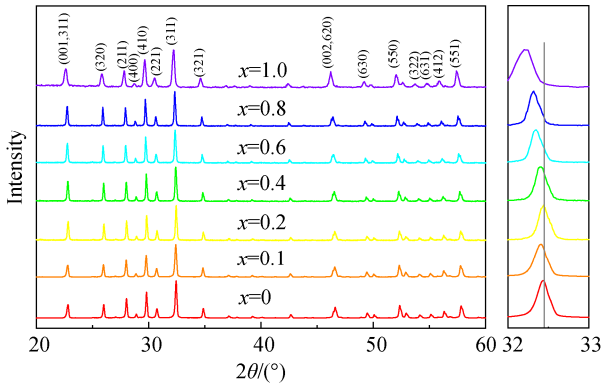
(c) Matrix and seed

Fig. 2 SEM images and XRD patterns of the matrix and seed powder obtained by the CMO and MSS methods.

interfacial energy was achieved by reducing the total interfacial area. The addition of salt created a liquid phase environment for particle growth during the high-temperature process. The morphology depended on crystal growth habits in the presence of a liquid phase. In light of this TTB structure, it was clear that the crystal grew faster along the [001] direction than in other directions. Therefore, multiple acicular NSN crystallites were observed, as shown in Fig. 2(b).

3.2 Microstructure development and densification

Fig. 3 shows the XRD patterns of ceramics prepared with different seed contents. All samples exhibited a single tetragonal tungsten bronze of NSN, and no second phase was detected. The intermediates ($NaNbO_3$ and $SrNb_2O_6$) were completely consumed in the process of synthesizing the matrix and reacted to form NSN. Further detailed XRD analyses were performed in the 2θ range 32° to 33°. It was found that all of the diffraction peaks shifted toward smaller 2θ values with increasing seed content. In this work, seed powder was synthesized through a facile ion (K^+ and Na^+) substitution approach in the Nb_2O_5+$SrCO_3$+NaCl+KCl system. These ion substitutions were incomplete, and some K^+ remained in the products[32]. Accordingly, we speculated that the residual K^+ caused lattice expansion due to the difference in ionic radii: $r(Sr^{2+})$=0.113 nm > r (Na^+)=0.139 nm. Lattice parameters were determined by the XRD patterns, as listed in Table 1. The unit cell volumes of NSN ceramics increased with increasing seed content.



(a) XRD patterns (b) Magnified image within 2θ=32°–33°

Fig. 3 XRD patterns of the NSN ceramics prepared with various seed contents

Table 1 Lattice parameters and densities of the NSN ceramics

Sample No.	ρ_a/(g·cm^{-3})	ρ_r/%	ρ_{th}/(g·cm^{-3})	a/nm	c/nm	Volume/nm^3
0NSN	4.444	88.1	5.044	1.232 3	0.3 888	0.590 33
0.1NSN	4.684	93.0	5.037	1.236 0	0.3 896	0.595 25
0.2NSN	4.682	92.8	5.035	1.236 1	0.3 896	0.595 42
0.4NSN	4.617	92.0	5.019	1.237 5	0.3 900	0.597 28
0.6NSN	4.589	91.8	4.998	1.239 2	0.3 906	0.599 81
0.8NSN	4.539	91.1	4.982	1.240 4	0.3 910	0.601 63
1NSN	4.333	86.8	4.991	1.257 4	0.3 873	0.612 30

Fig. 4 shows SEM images of ceramics prepared with different seed contents. It was found that seed content had a significant influence on the grain size distribution. It is well known that grain morphology depends largely on the particle-size distribution of the starting powder. As expected, when no seed was added (x=0), all the grains exhibited an equiaxed morphology. Numerous pores were evenly distributed on the ceramic surface. After adding seeds (x =0.1–0.8), large columnar grains were observed in the equiaxed grain areas, as shown in Figs. 4(b)–4(g). These columnar and equiaxed grains were interlaced. With increasing seed content, the percentage of columnar grains decreased, and the number and size of equiaxed grains increased. These results indicated that increasing seed content promoted the epitaxial growth of matrix particles. The number of pores increased with increasing seed content. As shown in Fig. 4(g), the columnar grains almost disappeared in the 0.8NSN sample. Fig. 4(e) shows a magnified image of the marked area in Fig. 4(d). Some equiaxed grains were distributed around the columnar grains, which is a distinctive trait of abnormal grain growth. With a further increase in seed content (x=1), only columnar grains with varied sizes were observed. These columnar grains were interlaced to form a loose structure. Plentiful pores were observed on rough surfaces.

Recently, the phase field simulation of grain growth has been widely reported[33]. Based on these theories, the microstructural changes of prepared ceramics with various seed contents may be explained. It is well known that the main driving force of sintering is the reduction of the surface free energy of an assembly of particles. The reduction of surface free energy was achieved by reducing the surface area. Competitive growth between starting particles reduced the total grain boundary area during the sintering stage. When no seed was added (x=0), competition only existed within the matrix powder. A fraction of the matrix grew into equiaxed grains by consuming nearby particles. The overall growth kinetics slowed once these grains "impinged". Thus, all grains showed equiaxial morphology, as seen in Fig. 4(a). With the addition of seeds ($0<x<0.4$), matrix growth competed with the seed-induced growth. The seeds rapidly developed into columnar grains by absorbing the surrounding matrix. The percentage of matrix decreased with increasing seed content, which greatly limited the growth of columnar grains. Moreover, the addition of seeds created more nucleation sites for the epitaxial growth of the matrix. Thus, with increasing seed content, the size and number of equiaxed grains continued to increase, and the grain boundaries became clearer. When the seed content exceeded the matrix content (x=0.6), only a small amount of seed grew into columnar grains. A large number of equiaxed grains are observed in Fig. 4(f). With a high level of seed content (x=0.8), it was difficult to find columnar grains in Fig. 4(g). When only seeds were used as raw materials (x=1), no matrix powder was consumed, and the growth of seeds was severely limited. The use of large seeds induced a weak driving force for sintering. Therefore, a loose structure is observed in Fig. 4(h).

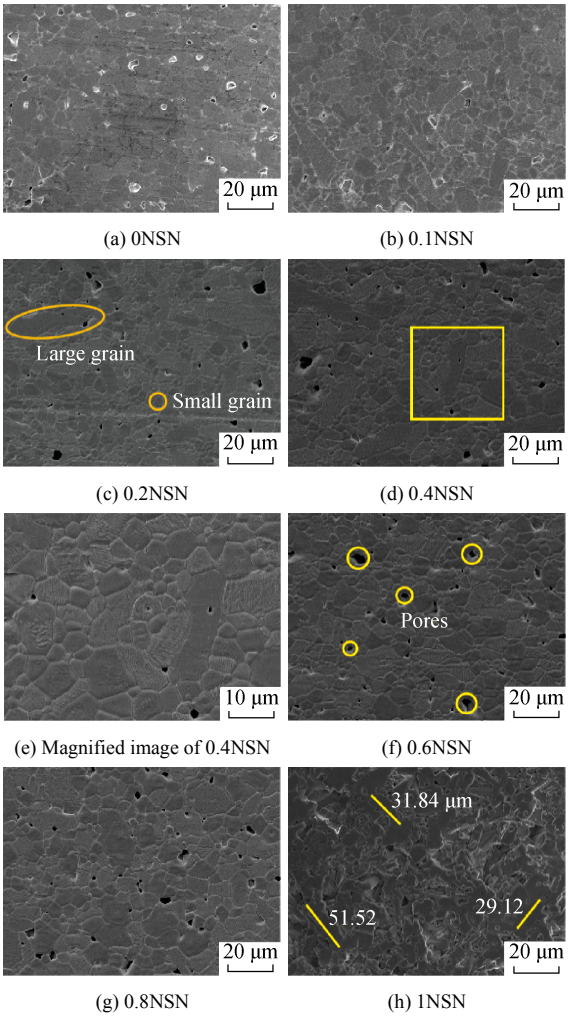


Fig. 4　SEM photograph of the NSN ceramics prepared with various $NaSr_2Nb_5O_{15}$ seed contents

The relative densities and photographs of ceramics prepared with different seed contents are shown in Fig. 5. All specimens were dense (>90%), except for the 0NSN and 1NSN samples. The results indicate that it was difficult to prepare dense ceramics using only matrix or seed powder as raw material. The densification of ceramics was promoted by the reaction sintering method and seed addition. This phenomenon may be explained by the random close packing of rigid particles. Random close packing is usually defined as a collection of particles packed into the densest possible amorphous configuration[34]. It has long been recognized that a higher packing fraction (φ) can be achieved by using collections of particles with a variety of sizes, in which case the packing fraction (φ) is defined as the ratio of the total volume occupied by spheres to the volume of the container. For spheres, the variation in size was usually

quantified by the polydispersity (δ) of the particle size distribution, i.e., the standard deviation of the radius divided by the average radius.

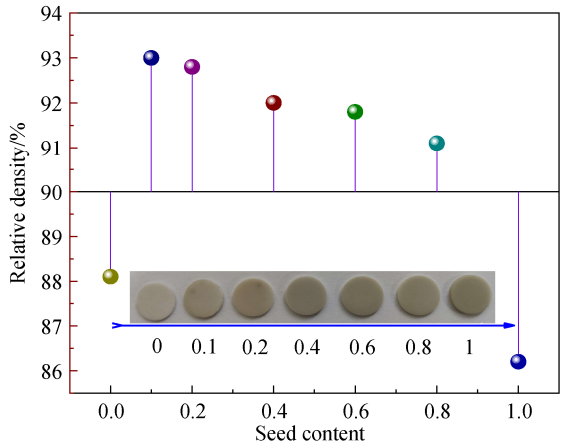
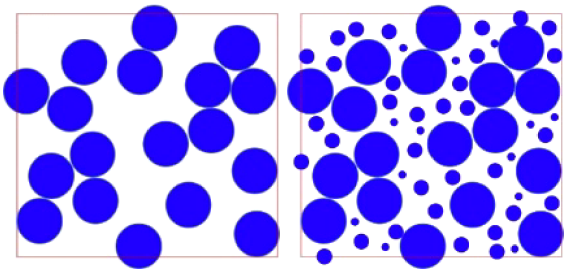


Fig. 5 Photographs and relative densities of the ceramics prepared with various $NaSr_2Nb_5O_{15}$ seed contents

A schematic diagram illustrating the random close packing of spheres with different polydispersities (δ) is shown in Fig. 6. Many voids are observed in the case of δ = 0. It is difficult to obtain a high-packing fraction (φ) using only a single size sphere. Prior studies found that the packing fraction (φ) of the densest random packing of monodisperse spheres (δ=0) was only 0.64[35]. Many experiments and simulations[36–37] have shown that increasing polydispersity (δ) greatly promotes an increase in the packing fraction (φ). In this structure (δ>0), large particles formed a skeleton, and the small particles packed more efficiently by fitting into the voids created between neighboring large particles, thereby increasing the packing fraction (φ) (Fig. 6(b))[38–39]. Essentially, the formation of ceramics was the result of the random packing of all grains. Therefore, we speculated that the densification of the ceramics may be related to the distribution of grain size.



(a) δ=0 (b) δ>0

Fig. 6 Schematic diagram illustrating random close packing with different polydispersities (δ)

3.3 Electrical properties of NSN ceramics

Fig. 7 shows the dielectric constant (ε) and dielectric loss (tanδ) as a function of temperature (–150 ℃ to 350 ℃) with different measurement frequencies (1–100 kHz). All samples exhibited two anomalies over the temperature range of interest. This phenomenon has been previously observed in many ferroelectrics with filled TTB structures[20]. The low-temperature anomalies corresponded to ferroelastic-to-ferroelectric phase (T_s) transitions, and the high-temperature anomaly corresponded to the ferroelectric-to-paraelectric phase (T_C) transition. All samples exhibited one broad dielectric peak I. With increasing frequency, T_s gradually increased. This was a distinctive trait of relaxor ferroelectrics. The T_s values for all samples were below room temperature. These results indicate that the local nanoscale areas of these samples were tetragonal phases at room temperature and became orthogonal phases below room temperature. These nanoscale areas promoted an increase in the degree of local disorder, giving rise to a diffuse phase transition at low temperatures. Moreover, the dielectric loss (tanδ) was found to be almost constant for all samples below the Curie temperature (T_C). In the high-temperature stage (T>T_C), the dielectric loss of these specimens markedly increased. The dielectric loss of ceramics is affected by various factors, and one of the main factors is the conductivity of ions. An increase in temperature resulted in an increase in ion conductivity, which led to a rapid increase in dielectric loss[19].

Fig. 7(h) shows the Curie temperature T_C and maximum dielectric permittivity ε_m as a function of seed content. It was found that T_C decreased linearly with increasing seed content. It is commonly known that the phase transition temperature of ferroelectric ceramics is closely related to the chemical composition[40]. As mentioned, the presence of a certain amount of K^+ in the ceramics could not be ruled out. The increase in seed content resulted in an increase in K^+ content at site $A1$, thereby weakening the degree of torsion of [NbO_6], reducing ion displacement, and giving rise to a decrease in Curie temperature. Compared with T_C, the maximum dielectric permittivity ε_m showed a more complicated trend with increasing seed content. ε_m reached a maximum value in the case of x=1. Generally, the volatilization of cations results in the formation of oxygen vacancies during the preparation of ceramics. These oxygen vacancies deteriorated the dielectric properties of ceramics. According to a previous report[41], ε_m was additionally affected by various factors such as internal stress, bulk density, domain density, and grain size.

The ferroelectric hysteresis loops of all specimens measured at room temperature are shown in Fig. 8. All samples exhibited well-saturated induced polarization. The P–E hysteresis loop became narrower with increasing seed content. With increasing seed content, the remnant polarization initially increased, reached a maximum (5.04 μC/cm^2) at x=0.1, and then decreased gradually. This can be explained by the presence of K^+ in the seed, as shown by the XRD analysis of Fig. 3. The specimen with 10%(mass fraction) seed showed the

optimum ferroelectric properties, with P_r=5.04 μC/cm^2 and E_C=12.734 kV/cm. The curve of the piezoelectric coefficient d_{33} as a function of seed content is plotted in Fig. 9. With increasing seed content, the value of d_{33} increased to a maximum value of 29 pC/N at x=0.1 and then gradually decreased. According to a previous report[42], d_{33} is generally expressed by the following relation:

$$d_{33} = 2Q_{\text{eff}}\varepsilon_0\varepsilon P \quad (1)$$

where Q_{eff} is the effective electrostriction coefficient

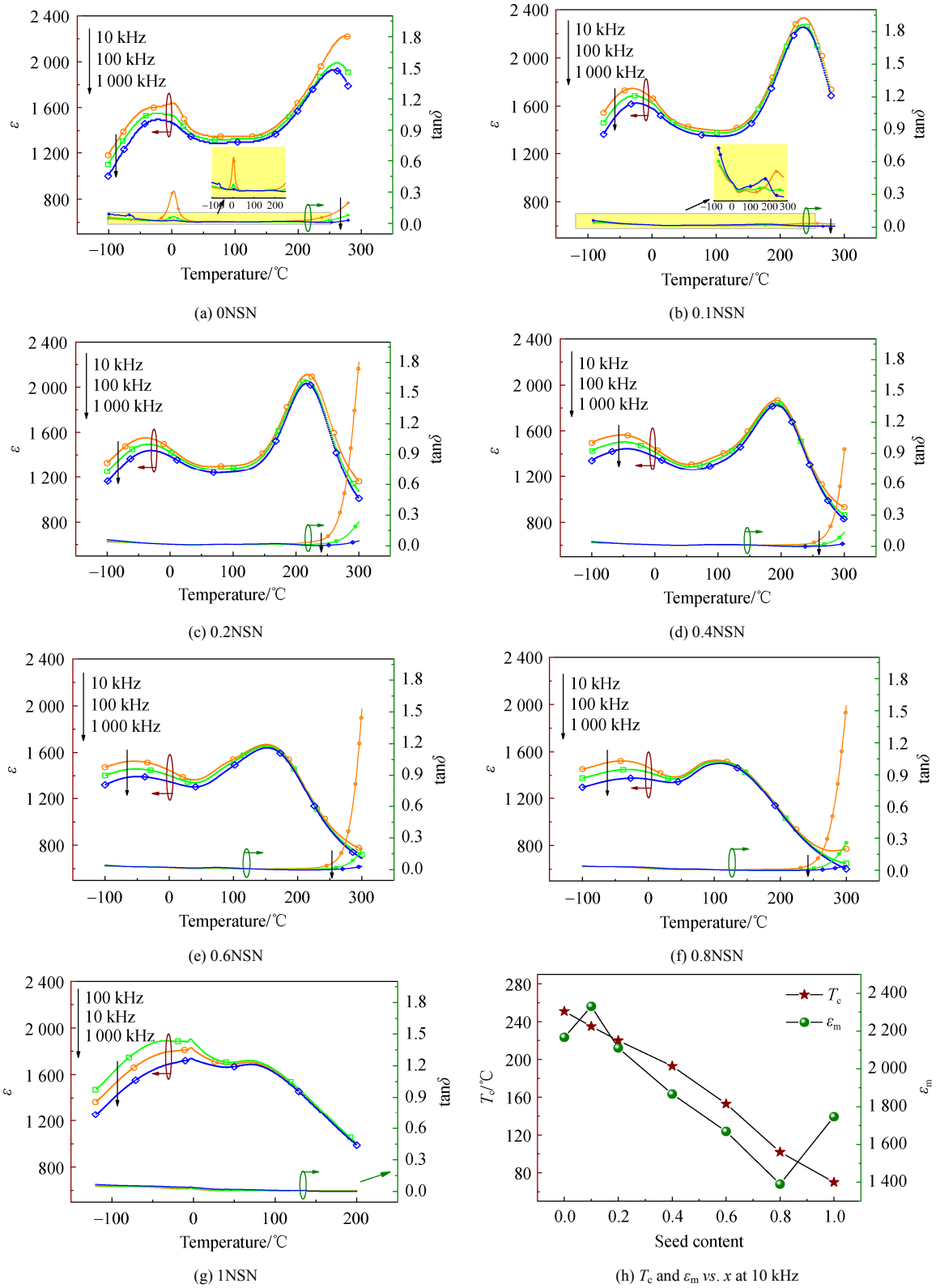


Fig. 7　Relative permittivity and loss tangent of the NSN ceramics as a function of temperature

related to the domain structure. The addition of seeds obviously cannot change the domain structure of ceramics. In this work, Q_{eff} could be considered a constant. Accordingly, the piezoelectric coefficient was dependent on the relative permittivity and polarization. The value of d_{33} exhibited the same change trend as that of εP. The above results indicated that the electrical properties of ceramics decreased (except for the 0NSN specimen with low density) with increasing seed content.

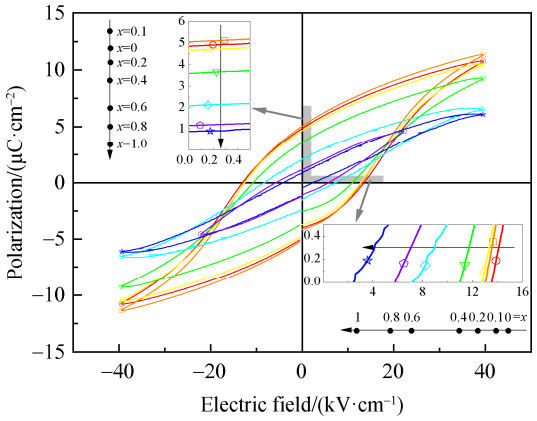


Fig. 8 *P*–*E* hysteresis loops measured at room temperature for the ceramics prepared with various $NaSr_2Nb_5O_{15}$ seed contents

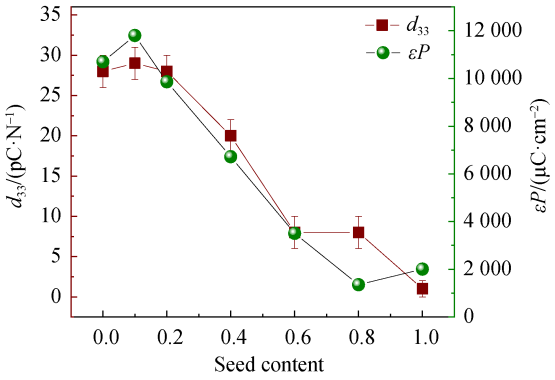


Fig. 9 Piezoelectric coefficients of the NSN ceramic as a function of $NaSr_2Nb_5O_{15}$ seed content

4 Conclusions

Dense NSN ceramics were successfully prepared by the reaction sintering method with addition of seeds. The raw materials (matrix and seed) were designed and synthesized by two routes, *i.e.*, conventional solid-state sintering and molten salt method, respectively. It was found that the addition of seeds had significant impacts on the densification and microstructure of the NSN ceramics. During reaction sintering, the seed played the role of nucleation point and promoted the epitaxial growth of matrix particles around it. The addition of large seeds was beneficial to the densification and regulated the microstructures of the NSN ceramics. This phenomenon could be attributed to the random close packing of raw material particles. The design of raw material is suggested as an effective way to prepare TTB-structured ferroelectric ceramics with high densities. This work also provides valuable technical parameters for the development of textured NSN ceramics in the future.

References:

[1] LV X, ZHANG X, WU J. Nano-domains in lead-free piezoceramics: a review[J]. J Mater Chem A, 2020, 8(20): 10026–10073.

[2] WU H, ZHANG Y, WU J, et al. Microstructural origins of high piezoelectric performance: a pathway to practical lead-free materials[J]. Adv Funct Mater, 2019, 29(33): 1902911.

[3] HAO J, LI W, ZHAI J, et al. Progress in high-strain perovskite piezoelectric ceramics[J]. Mat Sci Eng R, 2019, 135: 1–57.

[4] LI H, LI R, WANG G, et al. Microwave–fabrication and properties of NKN based lead-free piezoelectric ceramics Co-doped with CaO and B_2O_3[J]. J Chin Ceram Soc, 2020, 48(9): 1396–1404.

[5] WU J, XIAO D, ZHU J. Potassium-sodium niobate lead-free piezoelectric materials: past, present, and future of phase boundaries[J]. Chem Rev, 2015, 115(7): 2559.

[6] LI R, PU Y P, ZHANG Q W, et al. The relationship between enhanced dielectric property and structural distortion in Ca doped $Ba_2NaNb_5O_{15}$ tungsten bronze ceramics[J]. J Eur Ceram Soc, 2020, 40(13): 4509–4516.

[7] XU S D, DENG Z, SHEN S J, et al. Structural and electrical effects of Ag substitution in tungsten bronze $Sr_2Ag_xNa_{1-x}Nb_5O_{15}$ ceramics[J]. Ceram Int, 2020, 46(9): 13997–14004.

[8] HUO Z W, WANG H, XU J W, et al. Antiferroelectric behavior and giant strain in BNKT ceramics complex $Cs_2Nb_4O_{11}$ tungsten bronze phase[J]. Ceram Int, 2020, 46(8): 10067–10074.

[9] CAO L, YUAN Y, TANG B, et al. Excellent thermal stability, high efficiency and high power density of $(Sr_{0.7}Ba_{0.3})_{(5)}LaNb_7Ti_3O_{30}$-based tungsten bronze ceramics[J]. J Eur Ceram Soc, 2020, 40(6): 2366–2374.

[10] TAN Y, SHEN C, QIU T. Microwave dielectric properties of $(Ba_{1-a}Sr_a)_{4.8}(Sm_{0.7}La_{0.3})_{8.8}Ti_{18}O_{54}$ ceramics[J]. J Chin Ceram Soc, 2009, 37(6): 911–915.

[11] ROTARU A, MORRISON F D. Structural, electrical and relaxor properties of Sc–In solid solution in tetragonal tungsten bronze ceramics[J]. Ceram Int, 2018, 45(2): 2710–2718.

[12] OCHOA D A, CASALS J A, VENET M, et al. Dielectric and piezoelectric nonlinear properties of slightly textured lead barium niobate ceramics[J]. J Appl Phys, 2019, 125(2): 024101.

[13] LIU L, GAO F, HU G, et al. Effect of excess Nb_2O_5 on the growth behavior of $KSr_2Nb_5O_{15}$ particles by molten salt synthesis[J]. Powder Technol, 2013, 235: 806–813.

[14] LIU L, GAO F, HU G, et al. Fabrication of $KSr_2Nb_5O_{15}$ particles with high aspect ratio by two-step molten salt synthesis[J]. Adv Powder Technol, 2014, 25(1): 219–225.

[15] YANG Z, WEI L, CHANG Y. Preparation and morphology of anisometric KSr $_2Nb_5O_{15}$ particles[J]. J Eur Ceram Soc, 2007, 27(1): 267–272.

[16] TORRES-PARDO A, JIMENEZ R, GONZALEZ-CALBET J M, et al. Structural effects behind the low temperature nonconventional relaxor behavior of the $Sr_2NaNb_5O_{15}$ bronze[J]. Inorg Chem, 2011, 50(23): 12091–12098.

[17] HAO S L, LI J H, YANG P, et al. Enhanced electrical properties and

strong red light-emitting in Eu^{3+}-doped $Sr_{1.90}Ca_{0.15}Na_{0.9}Nb_5O_{15}$ ceramics[J]. J Am Ceram Soc, 2017, 100(12): 5620–5628.

[18] WEI L, HAN X, LI Z, et al. Fabrication of textured $Sr_2Na_{0.9}K_{0.1}Nb_5O_{15}$ ceramics: anisotropy in structures and electrical properties[J]. J Eur Ceram Soc, 2012, 32(14): 3773–3780.

[19] FAN J, YANG B, WEI L, et al. B-cation effect on relaxor behavior and electric properties in $Sr_2NaNb_{5x}Sb_xO_{15}$ tungsten bronze ceramics[J]. Ceram Int, 2016, 42(3): 4054–4062.

[20] YANG P, LI L, HAO S, et al. Electrical and transparent properties induced by structural modulation in $(Sr_{0.925}Ca_{0.075})_{2.5-0.5x}Na_xNb_5O_{15}$ ceramics[J]. J Eur Ceram Soc, 2017, 37(7): 2605–2613.

[21] WEI L, YANG Z, GU R, et al. The phase formation, microstructure, and electric properties of tungsten bronze ferroelectric $Sr_2NaNb_5O_{15}$ ceramics[J]. J Am Ceram Soc, 2010, 93(7): 1978–1983.

[22] LI L, YANG B, CHAO X L, et al. Effects of preparation method on the microstructure and electrical properties of tungsten bronze structure $Sr_2NaNb_5O_{15}$ ceramics[J]. Ceram Int, 2019, 45(1): 558–565.

[23] LIU L, GAO F, ZHANG Y, et al. Dense $KSr_2Nb_5O_{15}$ ceramics with uniform grain size prepared by molten salt synthesis[J]. J Alloy Compd, 2014, 616: 293–299.

[24] ZHANG T H, LIU Y G, ZHAO J Q, et al. Influences of protective atmosphere on the characterization and properties of $NaSr_2Nb_5O_{15}$ lead-free piezoelectric ceramics by sol–gel method[J]. Bull Mater Sci, 2015, 38(6): 1479–1486.

[25] YANG Y F, LIU Y Y, MENG J, et al. Preparation, structure and dielectric properties of $(Ba_{1-x}Sr_x)_2NaNb_5O_{15}$ ceramics[J]. J Alloy Compd, 2008, 453(1-2): 401–406.

[26] LIU L, GAO F, HU G, et al. Microstructure and electrical properties of potassium strontium niobate ($KSr_2Nb_5O_{15}$) ceramics[J]. J Alloy Compd, 2013, 580: 93–100.

[27] LIU L, GAO F, HU G, et al. Phase field simulation for the evolution of textured ceramics microstructure[J]. 2012, Ceram Int, 38(7): 5425–5432.

[28] SU S, ZUO R, LV D, et al. Densification and texture evolution of $Bi_4Ti_3O_{12}$ templated $Na_{0.5}Bi_{0.5}TiO_3$–$BaTiO_3$ ceramics: effects of excess Bi_2O_3[J]. J Alloy Compd, 2012, 519: 25–28.

[29] WEI L, YANG Z P, CHANG Y F, et al. Effect of seeding $Sr_2KNb_5O_{15}$ on the phase formation and microstructural development in reactive sintering of $Sr_2NaNb_5O_{15}$ ceramics[J]. J Am Ceram Soc, 2008, 91(4): 1077–1082.

[30] LIU L, GUO Z, WANG Y, et al. Synthesis and composition characterization of $K_{0.5}Na_{0.5}NbO_3$–$KSr_2Nb_5O_{15}$ ceramics[J]. Ceram–Silikaty, 2018, 62(3): 274–278.

[31] LIU L, GAO F, HU G, et al. Preparation of single crystalline $NaSr_2Nb_5O_{15}$ particles with acicular morphology[J]. Powder Technol, 2013, 246: 395–397.

[32] LIU L, GAO F, LI J, et al. Molten salt synthesis of acicular sodium strontium niobate particles[J]. Mat Sci Eng B-Solid, 2013, 178(20): 1359–1364.

[33] ZHANG Y, LIU L. Phase field simulation of template growth process in textured ceramics[J]. Model Simul Mater Sci, 2017, 26(1): 015008.

[34] DESMOND K W, WEEKS E R. Influence of particle size distribution on random close packing of spheres[J]. Phys Rev E, 2014, 90(2): 022204.

[35] RODRIGUEZ-ORTEGA J, ESQUIVIAS L. Structural Models of Dense Gels[J]. J Sol–Gel Sci Techn, 1997, 8(1–3): 117–123.

[36] HERMES M, DIJKSTRA M. Jamming of polydisperse hard spheres: The effect of kinetic arrest[J]. Europhys Lett, 2010, 89(3): 6.

[37] HUDSON T S, HARROWELL P. Dense packings of hard spheres of different sizes based on filling interstices in uniform three-dimensional tilings[J]. J Phys Chem B, 112(27): 8139.

[38] BROUWERS H J H. Erratum: Particle-size distribution and packing fraction of geometric random packings[Phys. Rev. E 74, 031309 (2006)][J]. Phys Rev E, 2006, 74(6): 1.

[39] CLUSEL M, CORWIN E I, SIEMENS A O N, et al. A 'granocentric' model for random packing of jammed emulsions[J]. Nature, 2009, 460(7255): 611–615.

[40] LV R, LIU L, WANG Y, et al. *A*-site cation and morphology control of $KSr_2Nb_5O_{15}$ microcrystalline by a modified molten salt method[J]. Adv Powder Technol, 2020, 31(8): 3256–3266.

[41] ZHANG C, GAO F, YAN X, et al. Effect of excess Sr^{2+} on the microstructure and electrical Properties of $KSr_2Nb_5O_{15}$ ceramics[J]. 2016, Ceram Int, 42(1): 242–250.

[42] SAID M, VELAYUTHAM T S, GAN W C, et al. The structural and electrical properties of $Sr_xBa_{(1-x)}Nb_2O_6$ (SBN) ceramic with varied composition[J]. Ceram Int, 2015, 41(5): 7119–7124.